Spectrum shape of K-orbital shakeoff electrons and accompanying nuclear beta particles. II. Decay of ^{147}Pm†

G. Schupp,* M. S. Freedman, F. T. Porter,‡ and D. A. Beery§
Chemistry Division, Argonne National Laboratory, Argonne, Illinois 60439
(Received 4 November 1976)

The composite K-orbital-shakeoff plus nuclear-electron spectrum was measured in coincidence with K x rays in the β emitter ^{147}Pm ($E_0 = 227$ keV) using the Argonne double-lens magnetic spectrometer and a Ge(Li) photon spectrometer. A bare NaI(Tl) scintillation electron detector allowed coincidence data to be recorded reliably down to an electron energy of ~ 5 keV. The measured spectrum showed prominently the expected intensity of Sm L-Auger lines at 5–6 keV following K x rays, and also the K internal conversion line of the 121.2 keV transition in Sm populated by the weak ($5.7 \pm 0.7 \times 10^{-5}$; $\log ft = 10.5$) inner β group of ^{147}Pm. Neither of these features was seen in earlier measurements. Corrections for the small contribution of the inner β group with its measured spectrum shape and intensity, and for the L-Auger peak were made. The resulting spectrum shape and the total K-ionization probability, $P_K = 8.7 \pm 0.7 \times 10^{-5}$, are both in good agreement with the K shakeoff theory of Law and Campbell, including a 9% contribution to the spectrum from K shakeup excitation. The spectrum shape agreement rejects a contribution to K ejection by the direct collision mechanism exceeding 60% of that due to shakeoff, compared with Feinberg's theoretical estimate of 21% and to earlier experimental indications. This latter evidence firmly rejects a recent proposal by Isozumi *et al.* which suggests a direct collision contribution equal to shakeoff to make up for their twofold lower shakeoff prediction.

[RADIOACTIVITY Measured electron spectrum in coin with K x rays in decay of ^{147}Pm; deduced shape and total K-ionization probability.]

I. INTRODUCTION

Probabilities for the ejection of atomic electrons during nuclear decays have been the subject of many recent experimental and theoretical investigations.[1] This particular study is concerned with the β decay of ^{147}Pm and the shape of the composite K-electron-plus-nuclear-electron spectrum observed in coincidence with K-shell excitation. It is the second[2] in a series of five such completed studies[3] undertaken to explore the effects of various parameters such as maximum β energy, atomic number, and deviations from allowed spectrum shape of the singles spectrum on the K-electron ejection process. The composite K-orbital–nuclear-β spectrum shape provides additional and in some ways more stringent tests of the theory of the process than is given merely by the measured ejection probability relative to normal β decay, P_K, and also has the possibility of indicating the separate contributions of different ejection mechanisms, as well as of discerning complicating effects such as internal conversion and Auger electrons and weak inner groups.

The principal orbital electron ejection mechanism is a one-step process in which the sudden change in the nuclear Coulomb field during nuclear β decay (rarely) causes ejection of K-shell electrons (and of outer orbital electrons with rapidly increasing probability with shell number). This process is referred to as shakeoff (SO) and is distinguished from the two-step process in which a nuclear β particle undergoes a final state Coulomb interaction with a K electron and ejects it from the atom. This latter direct collision (DC) process also occurs in principle but has generally a lower probability and a different associated electron spectrum shape. A third spectrum component, shakeup (SU), consists of the shaking process in which the atomic K electron is excited ($\Delta l = 0$) to some unoccupied bound state rather than ejected from the atom; thus it contributes only one (nuclear) electron to the spectrum in coincidence with K x rays, whereas SO and DC each contribute two. Bremsstrahlung photons accompanying β decay and other low intensity decay channels which give electron-photon coincidences were identified in the observed coincidence measurements by their characteristic distributions.

A study of the K-shakeoff spectrum accompanying the β decay of ^{143}Pr by Fischbeck *et al.*[2] (hereafter referred to as I) showed the desirability of using a magnetic spectrometer in studies of this type because distortions due to scattering processes commonly seen in solid state or proportional counter spectrometers, particularly at the lower energies important for the elucidation of the orbital ejection process, are much less severe. The ^{143}Pr study gave the first (thus far only) clear view

of the low energy orbital component, and also showed[1,2] the definite contribution of the destructive interference effect arising from the indistinguishability of the two free electrons in the final state, predicted by the theory of Law and Campbell.[4] Led by the above earlier work, this investigation used an improved electron detection system for the magnetic spectrometer, a new Ge(Li) spectrometer for photons, and a much more complete coincidence analysis system. The improved experimental arrangement allowed lower energy electrons which constitute the abundant orbital component and the interference term to be studied reliably. In spectrum shape studies, as contrasted to overall probability measurements, extreme care must be exercised if the resulting spectra are to distinguish between various theoretical predictions.

The study of ^{147}Pm was chosen as a complement to the ^{143}Pr work because it has a well established nearly allowed shape[5] with relatively much lower end-point energy and a nearby Z. The available energy parameter E_0 governs K SO in relation to the K binding energy B_K; for ^{143}Pr, $E_0/B_K = 21.4$, whereas for ^{147}Pm, $E_0/B_K = 4.9$. This lower value yields a much less pronounced separation of the main bodies of the nuclear and K-orbital overlapping continua (terms in SO theory described later) for ^{147}Pm, but a relatively much larger and more easily discerned contribution of the "indistinguishable-particle" interference term on the spectrum shape, and is therefore a more severe test of this recent[4,6] theoretical refinement. The same low E_0/B_K value leads to a prediction of a relatively much enhanced DC component, with perhaps improved chance of observing its influence on the spectrum shape. A comparison with earlier spectrum shape studies on ^{147}Pm by Stephas and Crasemann[7] and by Isozumi and Shimizu[8] using solid state and proportional counter spectrometers, respectively, was also thought to be desirable. In particular, neither of these earlier investigations showed any evidence for the K internal conversion or L-Auger electrons which are prominent features of this particular spectrum in coincidence with K x rays (see Fig. 6); this lack casts doubt on the validity of the conclusions inferred. In addition to the K internal conversion peak associated with the weak ($\sim 8 \times 10^{-5}$) decay branch[9] of ^{147}Pm to the 121.2 keV level in ^{147}Sm, the contribution to the K x-ray coincidence spectrum from this inner β group itself would also be expected to influence the spectrum shape. All these features were observed and corrected for in this study, which included a measurement of the intensity and spectrum shape of the inner group in coincidence with the 121.2-keV γ ray.

II. EXPERIMENTAL PROCEDURE

Investigations of this type push the usual β spectroscopic requirements and techniques to their limits in a variety of ways. Since K shakeoff is a low probability process ($\sim 10^{-4}$ per β decay for ^{147}Pm), intense sources, with attendant dead-time effects, must be counted over long times, requiring months long stability of the system to obtain, e.g., 1000 counts per each spectrum point. Several experimental compromises and intrinsic effects entail inefficiencies that require precise correction. Extreme source purity must be substantiated to avoid extraneous coincidences, and sources, although intense, must be thin to avoid scattering and spectrum shape distortions at low energies. Finally, the spectroscopic and electronic techniques must be valid to unusually low electron energies, $\ll B_K$, where the main part of the orbital SO component lies.

A. Source

The source was prepared by retarded ion beam deposition at 200 eV of mass 147 in an electromagnetic isotope separator onto a 50-μg/cm^2 carbon film supported over a 1-cm hole in 7-mg/cm^2 Al foil held on a 10-cm diam thin Al ring. Its mass thickness was <1 μg/cm^2; it was invisible in any illumination. It contained negligible ^{147}Sm after a preliminary separation of Pm on a cation column, judged also from the intensity of the analyzed mass beam at mass 148. No photon peaks other than from ^{147}Pm decay were detectable with a Ge(Li). The source strength was 18.6 ± 1.5 μCi; three independent measurements via the singles β count (in the spectrometer), the intensity of the K x rays and of the 121.2-keV γ ray, agreed within 10%.

B. β spectrometer

Figure 1 schematically shows the Argonne iron-free double-lens β spectrometer with the detectors and electronic circuitry used in this investigation. The spectrometer baffles were adjusted for 5% of 4π transmission and a nominal 5% momentum resolution, adequate for shape studies and involving only small resolution corrections.[10] In this mode the spectrometer induces[11] $<1\%$ spectrum distortions. The lens current and thus the momentum of the focused electrons is automatically controlled proportionally ($\pm 5 \times 10^{-5}$) by selecting the reference voltage for the control on a potentiometer. The convenient units for electron momentum are the potentiometer settings in millivolts (mV). Calibration of the spectrometer was based on the 193.658 ± 0.02 keV (Ref. 9) K-internal conversion line in the decay of ^{203}Hg, and on an internal standard,

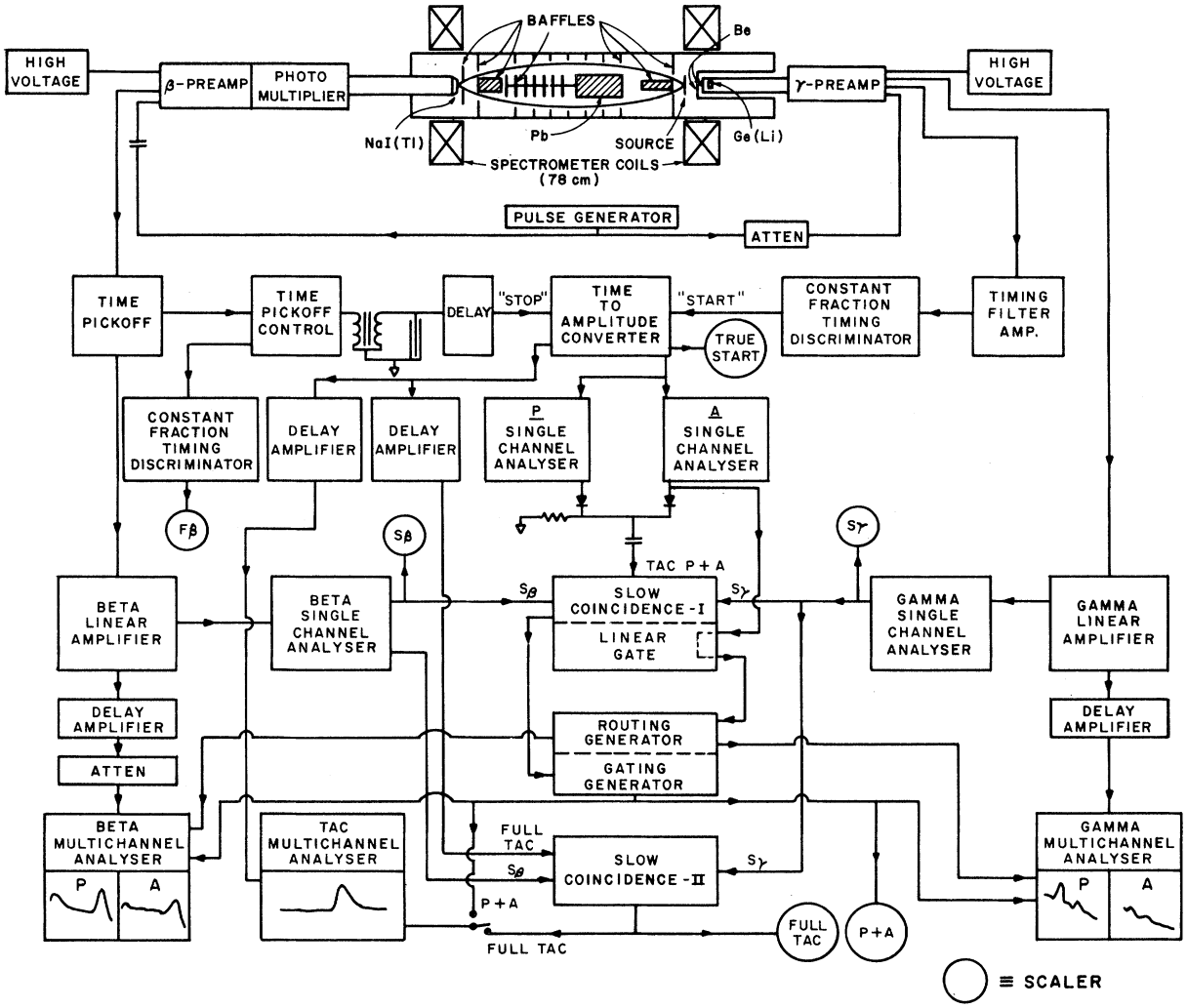

FIG. 1. Schematic diagram of apparatus and circuit. At top, double lens electron spectrometer with NaI(Tl) scintillation electron detector at left, and Ge(Li) photon detector at right of source mount. The fast-slow coincidence circuit used to gate the three multichannel analyzers which record the selected photon, photoelectron, and TAC distributions is described in the text.

the internal conversion line of the weak[9] 121.25 ±0.05-keV transition in ^{147}Sm. Daily monitoring of the residual earth's magnetic field inside the degaussing coils assured negligible effects by the residual field on electron focusing to <1 keV.

C. Electron detector

A bare, cleaved NaI(Tl) disk 12 mm in diameter and 1 mm thick was chosen as the electron detector for its superior scintillation efficiency[12] at low energy. A 10-mm diam detector baffle with rounded edges was 1 mm in front of the crystal. A 62-cm long, 2.5-cm diam Lucite light pipe led to a magnetically shielded RCA 8850 Quantacon photomultiplier tube located in a region of acceptably low magnetic flux. The system yielded approximately 0.7 photoelectrons per keV deposited in the crystal.

D. Photon detector

An Ortec Ge(Li) low energy photon spectrometer, 25 mm diam and 5 mm thick, with 40-μg/cm^2 dead layer, mounted in a 45-cm long 5-cm diam cryostat extension, inserted into a reentrant tube behind the source (20-mm gap; $\Omega_{h\omega} = 7\%$) in the β spectrometer. The extension and reentrant tubes each had a 0.047-g/cm^2 beryllium end window. The source-Be window distance was minimized con-

sistent with a $<1\%$ measured rise of the β spectrum at a low energy arising from electron backscattering. The energy resolution of the Ge(Li) system was 2.7 keV full width at half maximum for the 40-keV Sm $K\alpha$ x rays which were observed over a continuous bremsstrahlung spectrum. Near 40 keV the intrinsic efficiency is unity and for the 121.2-keV γ ray in ^{147}Sm, 0.50 ± 0.03, measured with a series of intensity-calibrated γ-ray sources.

E. Electronic circuitry

A fast-slow coincidence circuit gated three multichannel analyzers (MCA). The x-ray (photon) MCA gives the basic spectrum datum at each focused electron momentum, i.e., the intensity of the Sm K x rays [prompt (P) and chance (A) events recorded concurrently in separate MCA memory sections] in coincidence with electrons of energy selected by the magnetic spectrometer. The "β" and "time-to-amplitude converter" MCA records were used to determine the electron and fast-coincidence detection efficiencies and timing adjustments and as requisite checks on the number of P and A photon events. Various scalers recorded data used in the analysis.

The fast photon, focused electron coincidences were analyzed via a time-to-amplitude converter (TAC). The Ge(Li) drove the "start" pulse for the TAC. "True start" (TS) pulses, which account for start dead time losses, were scaled. The relatively slower rates for photon pulses (typically to 100/sec) compared with fast electron rates (up to 15 000/sec) gave TS losses of $<0.1\%$; much larger TAC stop losses are tolerable. The first photoelectron pulse from the Quantacon arising from each focused electron formed the "stop" input pulse to the TAC with a verified $>99\%$ efficiency. The short dead time of the negative, 50-nsec wide time pickoff (TPO) output logic pulse normally used for such timing applications introduced difficulties in the TAC operation. Repeated stop pulses coming from individually detected photoelectrons from a single scintillation event [$\tau = 250$ nsec for NaI(Tl)] spread the leading edge of the TAC peak with time-correlated "accidental" coincidences. To alleviate this problem, the positive output logic pulse from the TPO control was extended to 3.5 μsec and after inversion, shaping, and delay was used as the stop pulse to the TAC to prevent fast retriggering. The scaler recording "fast β rays" or stop pulses was driven with a similarly extended retriggering time so that its counts would match those of the TAC stop.

The time resolution of this system is a function of the energy of the electrons focused in the β spectrometer and is limited principally by the relatively slow 0.25-μsec decay time of the NaI(Tl) detector for single photoelectron pulses (cf. TAC efficiency discussion). True coincidences appear in a peak on the MCA-recorded TAC spectrum superimposed on a continuum of random coincidences. A TAC range of 0.5 μsec for electron energies above 25 keV (2 μsec below 25 keV) confined the true coincidence peak to less than half the channels on the TAC multichannel analyzer (MCA). A TAC output drove two parallel single channel analyzers (SCA) with precisely equal window-width settings, one selecting the region including the prompt (P) coincidence peak of the TAC spectrum, and the second selecting a timewise displaced segment of the accidental (A) coincidence spectrum. Thus true and chance coincidence rates were concurrently recorded. The joined outputs from the P- and A-SCA's provided the TAC input into one of two slow triple coincidence circuits (I): The full TAC output fed the other (II). The decoupled signal from the A SCA was used for routing the accidental events into a selected memory segment of the γ and β MCA's.

An amplified linear signal from the photon detector through a SCA with a pulse shape discriminator provided the slow γ (S_γ) coincidence requirement, differentially selecting only that portion of the photon energy spectrum of interest. This range included also the 121.2-keV γ ray in ^{147}Sm, so that the shape of the weak inner β group from ^{147}Pm could be measured concurrently with the SO shape, via the intensity of the γ ray.

The electron side was similar except that the β SCA driving the slow coincidence inputs rejected only low amplitude pulses. At all electron energies incident on the NaI(Tl) crystal there is a very broad range of pulse amplitudes extending down to single photoelectron events due to backscattering of a fraction of the focused electrons from the crystal, which thus deposit only a portion of their energy. Due to the large dynamic range of the pulses from the β preamplifier and the need to see even single photoelectron events, the photomultiplier voltage and the linear amplifier gain used were sufficient to saturate the amplifier for all scintillation events releasing more than about 10 photoelectrons. The β SCA (S_β) discriminator was set precisely beyond the upper amplitude limit of the single photoelectron-event distribution. These were rejected for higher focused electron energies (≥ 10 keV) since the decay of the prolifically populated delayed states[12] in NaI(Tl) gives many single photoelectron events which would have drastically increased the chance coincidence rate. This mode of slow coincidence operation was labeled "triples" (S_γ, S_β, TAC). For electron energies below 10 keV the S_β requirement was removed in both of the slow

coincidence circuits (labeled "doubles"; S_γ, TAC), because relatively fewer delayed states are formed, and one can achieve higher β efficiencies by accepting the substantial fraction of low energy focused electrons which give only a single photoelectron.

Pulse height distributions for electrons and photons which satisfied the coincidence requirements were recorded on separate multichannel analyzers (β and γ MCA's), gated by the slow coincidence output. Both analyzers were operated in a split memory mode such that prompt events (in the P SCA window) were stored in one-half of the β and γ MCA's, respectively, while events falling timewise in the A-SCA window were routed into the other half of the respective MCA's.

The second slow triple coincidence circuit (II) gave the usual coincidence gate for the TAC MCA. Thus the TAC analyzer recorded the *full* TAC distribution for which all coincidence requirements had been met. For the daily check on the channel positions and widths of the P- and A-SCA windows on the TAC spectrum, the TAC analyzer was gated by the (I) slow coincidence circuit. These window positions were measured quickly and accurately by generating high chance rates by setting the TAC range at its maximum of 80 μsec and lowering the γ discrimination level on the TAC start pulses into the noise. Analyses of the TAC spectrum for each electron momentum setting afforded a check on the number of true coincidences obtained in each run and a means for determining the coincidence (or TAC) efficiency.

III. DATA ANALYSIS

The composite *electron* momentum spectrum measured in coincidence with K x rays was taken as the corrected *K x-ray coincidence rate* per unit electron momentum, i.e., per mV,[13] as a function of the focused electron momentum expressed in mV.[14] Thus the principal datum used in the analyses for each mV setting of the spectrometer current control was the K x-ray intensity derived from the coincidence-gated photon MCA. Analyses of the TAC and β MCA data were used in making various corrections to the observed x-ray rate. Figure 2 shows examples of the type of data collected at each of the 50 momentum settings of the spectrometer used in the coincidence runs.

A. X-ray photopeak rate

The true coincidence photon spectrum shown in Fig. 3(a) was obtained from channel-by-channel P-A differences of Fig. 2(a) for a spectrometer setting of 230 mV (~31.7 keV). The Sm K x-ray peaks

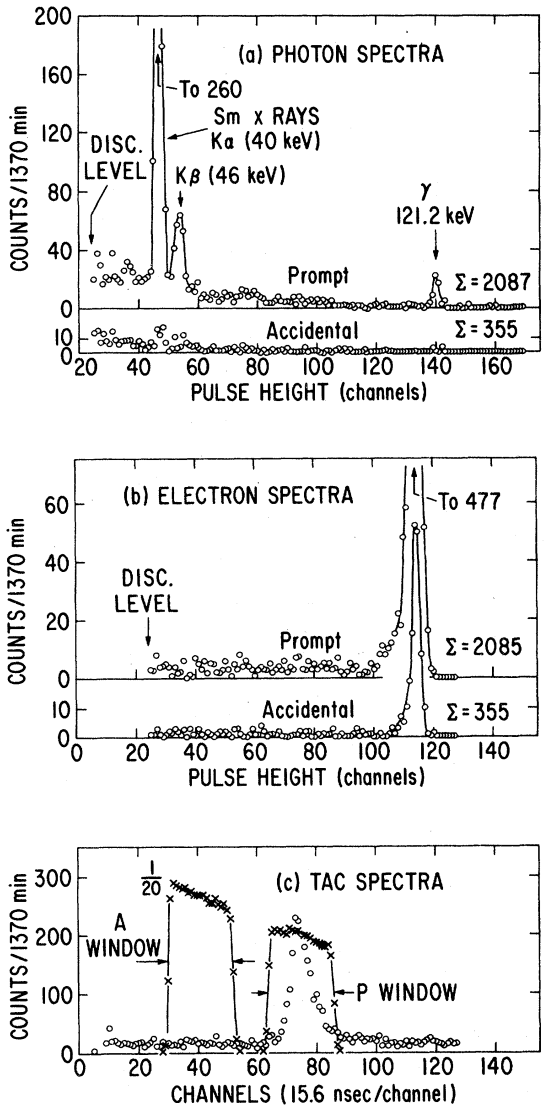

FIG. 2. A sample set of raw data from the three multichannel analyzers for the run on ^{147}Pm at 230-mV spectrometer potentiometer setting (31.7 keV focused electron energy). The data points from the prompt and accidental sections of the MCA memories are folded to superpose corresponding channels for both the photon and electron spectra. In the photoelectron amplitude spectrum (b), the peak at channel 114 is due to amplifier saturation for pulses having 10 or more photoelectrons. The discriminator level was set to reject the strong single photoelectron peak. The TAC spectrum shows the prompt coincidence peak (channel 73). The cross points show the spectrum of accidental coincidences generated at an artificially high rate in a separate measurement made to delineate the channel widths of the accidental (left) and prompt (right) single channel analyzer windows selecting TAC output pulses (see text). The exponentially decaying slope of the tops of the P and A window tests is due to the high random stop rate.

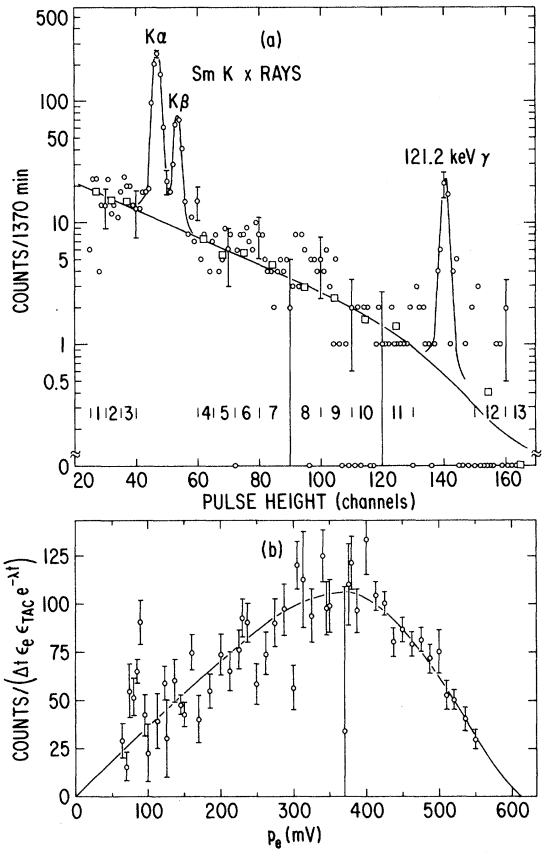

FIG. 3. (a) Photon coincidence spectrum (prompt minus accidental) from data of Fig. 2. Open squares show smoothed averages of each channel group (groups indicated below), on background continuum, each obtained from separate plots of group-average value vs mV [e.g., Fig. 3(b)]. Curve (least-squares fit to square points) was used as continuum under photon peaks. (b) Photon count rate in group 3, (channels 35–39), corrected for electron detection efficiency, TAC efficiency, and ^{147}Pm decay, plotted vs focused electron momentum in mV units.

in coincidence with the electron SO spectrum were superimposed on a continuum which arose from internal and external bremsstrahlung in coincidence with the normal β spectrum as well as from the Compton distribution of the 121.2-keV γ ray in coincidence with the weak inner β group. To reduce the statistical uncertainties in determining the photon continuum beneath the x-ray peaks for each coincidence run, the intensity and shape of the continuum was assumed to vary smoothly as a function of mV, so that the fluctuations of background continuum shape for any one mV setting could be smoothed by correlating data from all mV settings. Channels on the photon continuum above and below the x-ray peaks were grouped (5–10 channels per group) and the intensity of each of 13 groups plotted as a function of mV, e.g., Fig. 3(b). A smooth curve through the points yielded average coincidence rates at the center of each group as a function of mV. Then, at each mV, a quadratic curve was least-squares fitted to these group average rates to give interpolated background rates to be subtracted from the channels summed for the $K\alpha$ and $K\beta$ peaks. Attempts to fit theoretical internal bremsstrahlung distributions to the continua had some success but it was thought that the empirical approach was more appropriate.

The $K\alpha + K\beta$ sum rate then was corrected for a variety of instrumental losses and for the contribution of the weak decay branch to the 121.2-keV level in ^{147}Sm. This latter decay is in coincidence with K x rays which follow K internal conversion of the 121.2-keV transition, as is the K conversion electron line itself. An average value for the $K\alpha/K\beta$ ratio of 3.85 ± 0.07 was determined from these analyses which showed no systematic variation with electron momentum. The literature value[15] for this ratio is 4.0.

B. Energy-dependent electron detection efficiency

The usual way of determining the efficiency of the electron detector by extrapolating the true coincidence electron pulse amplitude distribution to zero pulse height, thereby estimating the fraction of counts lost below the discrimination level at each mV setting[16] is inadequate at the low electron energies of interest in SO studies. A new technique, used here, was developed for the study of ^{151}Sm, which has a maximum energy of only 28 keV for its K SO spectrum. Details will be given in Paper III of this series. It involves use of the Quantacon photomultiplier, with which discrete amplitude peaks corresponding to the release of one, two, etc., photoelectrons from its photocathode can be seen (as in Fig. 4). By computer construction the amplitude distributions of analyzed pulses corresponding to two, three, etc., photoelectron events emitted in the decay of the prompt (250 nsec) scintillations from NaI(Tl) were calculated. This was done using a convolution procedure based on an observed single electron distribution and a measured time-interval response function of our linear amplifier, gated electron MCA combination. Computer assisted deconvolution of the photoelectron pulse amplitude distributions observed at each focused electron momentum yielded the fraction of pulses resulting in one, two, three, etc., photoelectron events. From these fractions the fraction of focused electrons giving *zero* photoelectrons was obtained by a Poisson fitting procedure.

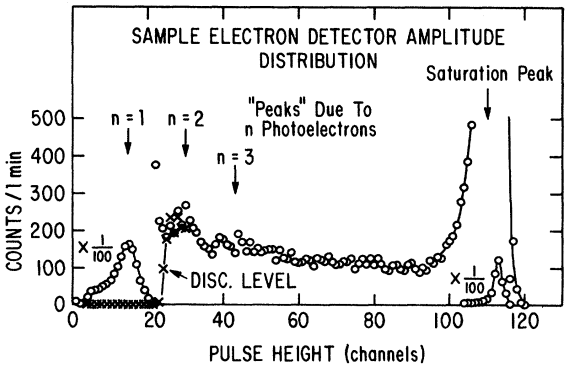

FIG. 4. Pulse amplitude distribution from electron detector obtained by focusing 31.7-keV electrons (230 mV) in magnetic spectrometer as in Fig. 2. Peaks corresponding to groups of 1, 2, or 3 photoelectrons ejected from photomultiplier photocathode are marked, as well as the amplifier saturation peak due to 10 or more photoelectrons. Circles are singles counts (no coincidence gate on MCA) minus background. Crosses are "self-gated" singles (only gating requirement is electron amplitude above "one-electron peak"; discriminator at channel 24), also minus background. Such distributions were measured for purpose of determining electron detection efficiency (see text) at each focused momentum.

In doubles where all single electron pulses were accepted (no S_β coincidence requirement) the fraction of "zeros" constituted the total detection inefficiency; the efficiency decreased from 0.90 at 10 keV to 0.53 at 3 keV. In the triples mode, with the S_β discriminator just above the "one-electron" level, the loss of all zeros and "ones" was augmented by the fraction of each of the deconvoluted components, i.e., "twos, threes, and fours," that lay below the selected S_β discrimination level, giving an efficiency function decreasing from 0.94 at 160 keV to 0.80 at 10 keV. The detection efficiency is reliable down to ~5 keV.

Figure 4 shows the pulse height distribution in the singles and self-gated modes. The intense peak in singles at low pulse heights was caused by one-photoelectron pulses arising principally from the numerous long-lived trapping states in NaI(Tl) generated by each focused electron of moderate-to-high energy. The triples discrimination level is shown by the singles spectrum self-gated by those pulses rising above the one-electron level. The intense saturation peak is also seen. The saturation pulse was kept on scale so that the sum of all MCA coincidences could be used as a check on the electronic system and on the photon P-A coincidences.

C. Coincidence efficiency and accidentals correction

Fast coincidence losses resulted when true coincidence pulses in the TAC spectrum fell outside the prompt (P) SCA window setting. Figure 2(c) shows the complete TAC spectrum obtained for the run at 230 mV. Superimposed on the TAC spectrum is a check (accidentals) run taken to show the P- and A-SCA windows. The leading (left) edges of the TAC peaks, produced by the photon start pulse, were generally well defined and steep. When necessary, corrections were made for losses on the leading edge by calculating the small fraction of the peak area lying to the left of the lower window edge of the P-SCA.

Estimation of the fraction of true coincidences falling above the upper edge of the P-SCA window by simple graphical extrapolation of the tail of the TAC peak was difficult, however, because of the tailing distribution and the uncertainty in the accidental continuum. To estimate these losses reliably, the shape of the right side of the TAC peak was calculated (Fig. 5) from the distribution of arrival times of the first photoelectron pulse in each scintillation event, since the TPO unit generating TAC stops was adjusted to be sensitive to over 99% of single electron pulses. The time spread arises from the prompt nearly exponential fluorescence mean decay time of the NaI(Tl), ~250 nsec.[17] (The TAC peak width is purely instrumental, since the K vacancy lifetime in Sm is $\sim 10^{-16}$ sec.) At each focused electron energy the observed electron amplitude distribution was analyzed into a composite sum of multielectron events, as noted. For each n-electron component the probability for arrival of the first photoelectron goes as $P(t) \propto e^{-nt/250}$, t in nsec, i.e., each component gives an exponential term of decay time $250/n$ nsec as illustrated in Fig. 5. By taking $t = 0$ at the TAC peak, the fraction $(fl)_n$ of TAC events lost beyond t_w, the upper P-SCA window edge, is, for each n electron component,

$$(fl)_n = e^{-nt_w/250}.$$

Summed over all n electron events, with weighting factors f_n (from the ϵ_{elec} analyses), at each focused electron energy, the total TAC loss is then

$$(FL) = \sum_n f_n e^{-nt_w/250}.$$

This is illustrated in Fig. 5, for 90 mV, for which the (typical) TAC efficiency was 0.92.

Possible causes of an incorrect P-A subtraction in the photon or electron analyses included unequal P and A window widths, TAC nonlinearity, and TAC stop slope. The P and A window widths were monitored and set before and after each run to 1%

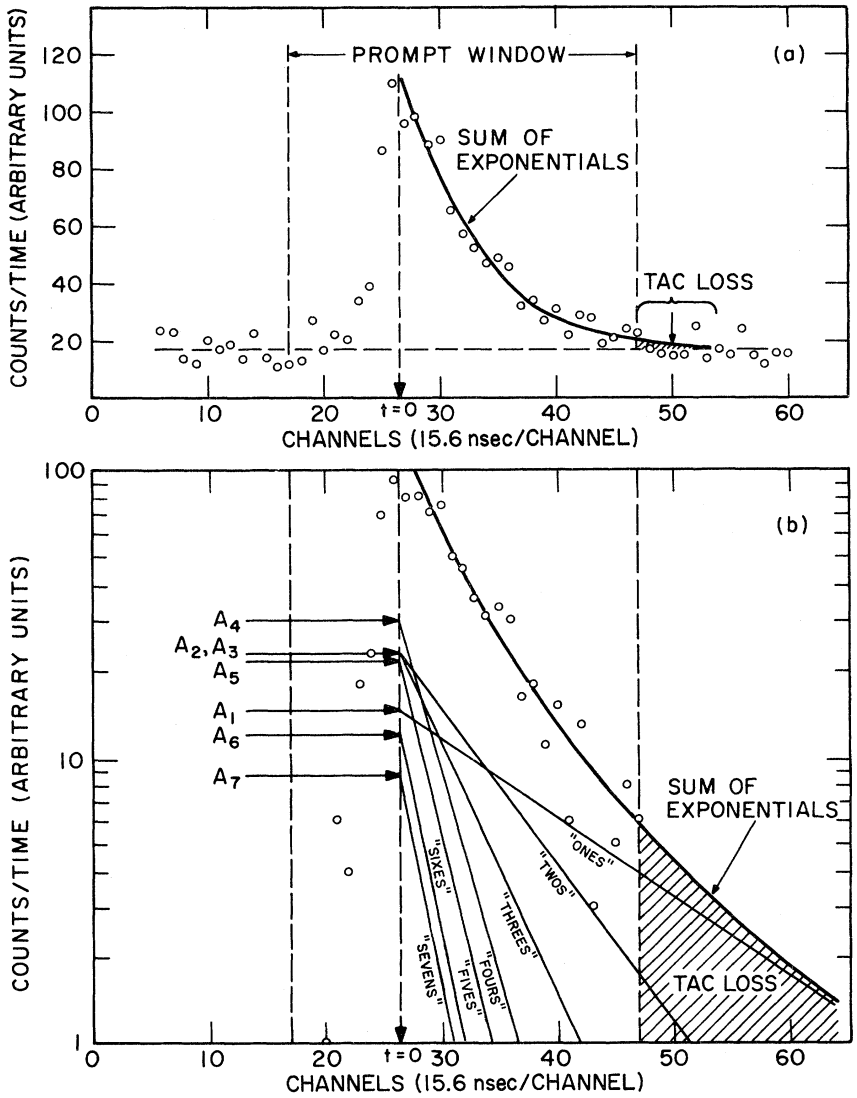

FIG. 5. Curves for determining TAC (coincidence) efficiency; a set of such curves is needed for each focused electron momentum. Curves show prompt coincidence peak, minus accidentals, in relation to prompt single channel analyzer window; ordinate of curve (a) is linear, and of (b), logarithmic. Curve (b) shows exponentially decaying n-electron-group components of prompt peak, where n is number of photoelectrons in any event. The components of the focused electron amplitude distribution, each with relative intensity $\propto A_n$, are determined by deconvoluting that distribution. The fraction of area under each exponential component lying to right of upper prompt window edge is its inefficiency; their weighted sum is the TAC inefficiency.

[Fig. 2(c)] and corrections made when necessary to compensate small drifts. The TAC nonlinearity was observed to be less than 1% over the used span. A high stop rate (mean pulse spacing of the order of the TAC range) of random pulses produces an exponentially decaying TAC slope (cf. check run, Fig. 2). The actual experiment, however, showed no detectable slope over a 2-μsec TAC range (calculated $<1\%$) and no correction was made.

D. Dead-time corrections

The low coincidence rates inherent in this type of experiment require that the singles counting rates be relatively high, particularly of electrons. Photon rates may also be high depending upon the character of the photon spectrum and how near to the noise level the discriminator must be set to avoid x-ray losses. Corrections were made for those dead-time losses that exceeded the 1% level.

1. Fast coincidence dead-time losses

Fast coincidence losses as great as 1% occur only as true start losses in the TAC. The measured TAC-start dead time is (5 μsec + TAC range). The dead-time correction was based on recorded true starts.

2. Slow coincidence dead-time losses

These may occur in the β and photon SCA's and in the MCA's; only the first exceeded the 1% level. To prevent spectrum pileup distortion, even the β SCA pulses below the discriminator level intentionally extend its dead time following an analyzed pulse.

The loss rate in S_β analyzed and recorded coincidences was measured for a 60-Hz pulser, mixed with β pulses into the β preamplifier, and also inserted into the photon preamplifier (pulser only), as a function of the focused β pulse rate and energy. This test yielded a β SCA dead-time τ fitting an extending dead-time model $N_{\rm obs} = N_t \exp(-N_t\tau)$. The electron energy affects the loss rate owing to the increase with focused electron energy in the single electron pulse rate from long lived states in NaI(Tl). (In fact this high rate of delayed state single electron pulses was observed to stretch out the pulse length of high energy saturated pulses up to 40 times that of unsaturated pulses.) Since the true rate N_t in the exponential loss factor must include pulses below the slow β (S_β) discriminator level, the *fast* β rate $N_{(f\beta)}$ from the TPO which included all single electron pulses was found to be a proper measure of the total pulse rate into the β SCA to account for the pulser rate loss, so we have instead,

$$N_{{\rm obs}(S_\beta)} = N_{t(S_\beta)} \exp(-N_{(f_\beta)}\tau).$$

The slow β dead-time losses ($\leq 7\%$) were applied to both coincidence and singles spectra.

E. Routine system monitors

A pulser fed to both the photon and electron preamplifiers was used to monitor the electronic system daily, testing all coincidence operations and all three MCA's for overall system stability. Sums of the recorded P and A events were compared separately for the photon and electron analyses of each run (required 1% match). The spectrometer current control was checked (and reset to 10^{-5}) daily, as also were the vacuum and degaussing field. Photon and electron emission rates from the source were measured daily at preselected energies, checking the mechanical stability of the source and the source decay (6.5%) during the three months running time of this experiment.

F. Calculation of experimental momentum distributions

Finally, small corrections significant for only the four highest energy points for finite spectrometer resolution[16] were applied to the singles and coincident momentum spectra. The composite K x-ray coincidence spectrum (Fig. 6) includes several significant contributions: shakeoff, shakeup, and direct collision ejection in the ground state β transition; the weak inner β decay branch itself seen via K x ray following K conversion of the 121.2-keV transition in ^{147}Sm, and also its equally intense associated K internal conversion line (inner group SO is negligible); and L-Auger electrons which follow only $K\alpha$ x rays. M-Auger electrons, which follow $K\beta$ x rays are <1.5 keV. Also shown is the momentum spectrum of the inner β group in coincidence with the 121.2-keV γ ray. The relative intensities (areas of continuous or line components of the momentum spectrum) in the coincidence and single spectra used to obtain P_K and the shaking spectrum shape, are given by

$$I(\text{singles}) = N_0\Omega, \tag{1}$$

$$I(\text{SO}; K_x(\text{SO})) = 1.93 N_0 P_K \Omega \omega_K \epsilon_{Kx}, \tag{2}$$

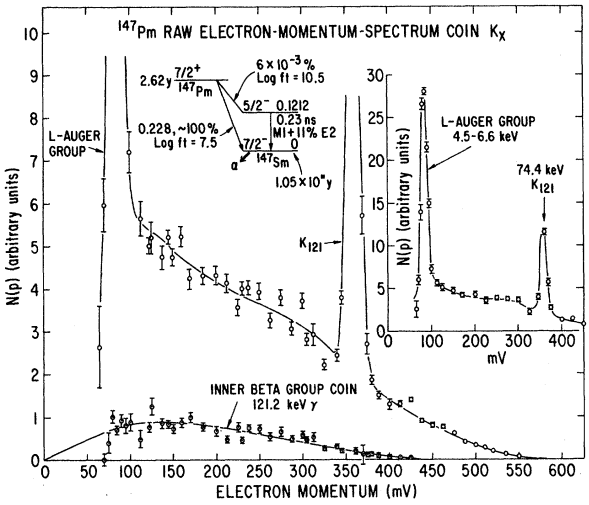

FIG. 6. The total electron momentum spectrum of ^{147}Pm in coincidence with Sm K x rays, corrected for all losses, detection efficiencies, and sample decay. The continuous distribution includes the K shaking and direct collision contributions as well as the weak inner β group in ^{147}Pm decay (see decay scheme), seen in coincidence with K x rays following K internal conversion of the 121.2-keV transition. The K_{121} conversion line, and the unresolved L-Auger group appear as superposed lines (see inset). Below is shown the inner group spectrum in coincidence with the 121.2-keV γ ray, in (approximately) the correct relative abundance to the total, K x-ray coincidence spectrum.

$$I(K\text{ line}; K_x(\text{IC})) = N_0 f \Omega [\alpha_K/(1+\alpha)]\omega_K \epsilon_{Kx}, \quad (3)$$

$$I(\text{inner}\,\beta; K_x(\text{IC})) = N_0 f \Omega [\alpha_K/(1+\alpha)]\omega_K \epsilon_{Kx}, \quad (4)$$

$$I(\text{inner}\,\beta; 121\gamma) = N_0 f \Omega [1/(1+\alpha)]\epsilon_{121}, \quad (5)$$

$$I(L\text{-Auger}; K\alpha_x(\text{SO})) = N_0 P_K \Omega \omega_K \epsilon_{Kx}\{\nu\}, \quad (6)$$

where

$$\{\nu\} = \frac{K\alpha_2}{K_x}(1 - \omega_{L2} - f_{23}) + \left(\frac{K\alpha_1}{K_x} + f_{23}\frac{K\alpha_2}{K_x}\right)(1 - \omega_{L3})$$

and

$$I(L\text{-Auger}; K\alpha_x(\text{IC})) = N_0 f[\alpha_K/(1+\alpha)]\,\Omega\omega_K \epsilon_{Kx}\{\nu\}. \quad (7)$$

$I(x; y)$ represents the intensity of the x electron group in singles or in coincidence with photon y, except that SO represents shakeoff plus shakeup and direct collision; N_0 is the ^{147}Pm decay rate; Ω is the transmission-resolution product for the magnetic spectrometer[16]; and f is the very small inner group branching ratio (5.7×10^{-5}). K_x(SO), $K\alpha_x$(SO), K_x(IC), and $K\alpha_x$(IC) represent K(total) and $K\alpha$ x rays resulting from shakeoff (SO) and internal conversion (IC), α_K and α are the K-shell and total internal conversion coefficients for the 121.2-keV transition, ω_i is the fluorescence yield of the ith (sub) shell and ϵ_{Kx} and ϵ_{121} are the overall detection efficiencies for the K x ray and 121.2-keV γ ray, respectively; $K\alpha_1$ and $K\alpha_2$ denote KL_3 and KL_2 transitions, and f_{23} is the Coster-Kronig yield between the L_2 and L_3 subshells. The 1.93 factor in Eq. (2) is the average number of electrons emitted per K-shell shaking plus direct collision event (2 for SO and DC and 1 for SU) evaluated from Law-Campbell[4] theory; $P_K(\text{SU})/P_K(\text{SO}) = 0.089$ and $P_K(\text{DC})/P_K(\text{SO}) = 0.206$ for ^{147}Pm; $[2(1+0.206) + 0.089]/1.295 = 1.93$. Justification for the intensity of the direct collision (DC) contribution will be discussed later.

IV. RESULTS AND DISCUSSION

A. Singles spectrum

Equation (1) represents the singles β-ray spectrum. While the ensemble of slow β scaler values from the individual runs on the coincidence data points gave a singles spectrum, better results from a special short singles run are shown in Fig. 7. This was taken with the slow β discriminator set just above the upper end of the two- (rather than one-) electron distribution from the β detector to avoid spectrum pileup distortions from single photoelectron events from NaI(Tl) delayed states. There was evidence of such distortions; the singles electron distribution showed a small *excess* two-electron peak as well as a strong excess one-electron peak with respect to the electron distribution observed in coincidence with K x rays. Electron detection efficiencies and dead-time corrections were determined as for the coincidence runs. Figure 7(a) shows the Kurie plot and Fig. 7(b) the shape plot (ratio of experimental points to those calculated for an allowed spectrum shape with end-point energy of 227.5 keV).

This singles spectrum does not follow the allowed shape of most earlier measurements[5] and the measured end point is 3 keV higher, at 227.5 keV. The inset of Fig. 7(a) shows a momentum plot of the K internal conversion line of the 121.2-keV transition, taken in coincidence with Sm K x rays, as an internal calibration standard. It has the width and shape of the strong K-conversion line

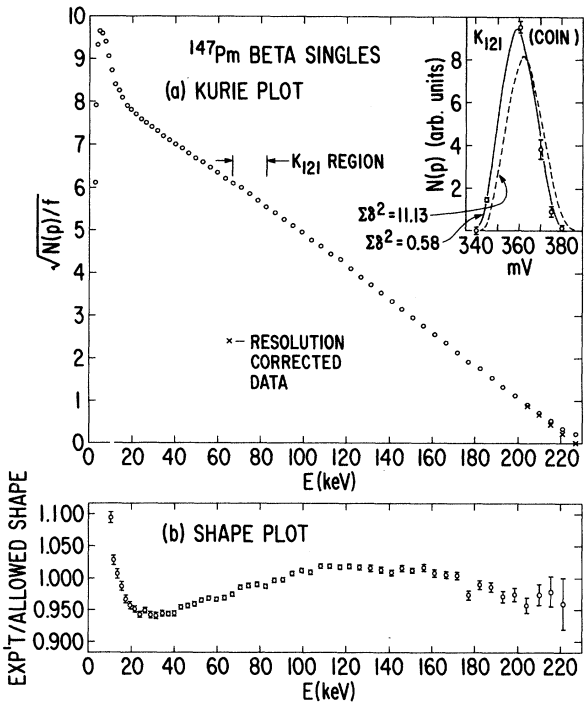

FIG. 7. ^{147}Pm β singles spectrum. (a) Kurie plot. Inset: momentum plot of the very weak (3×10^{-5}/decay) K_{121} conversion line internal standard (solid curve), observed in coincidence with K x rays. Data peeled from Fig. 6. Dashed line with centroid position at 362 mV would give calibration that would yield $E_0 = 224.5$ keV for Kurie end point. Residuals sum from Gaussian line fits to data points marked for each line. Cross points above 200 keV show data corrected for magnetic spectrometer resolution; circles show uncorrected data. (b) Shape factor plot (experiment/theoretical allowed shape) for $E_0 = 227.5 \pm 1.0$ keV.

of ^{203}Tl and other isotopes similarly deposited, observed in singles and in coincidence at the same spectrometer settings and has the same calibration constant. The line at 362 mV shows where the line centroid would have to lie in order for the singles β spectrum end point to be 224.6 keV, the average of earlier end-point determinations.[9] The much larger sum of residuals (marked on lines) from a fit of the shape of a ^{203}Hg K conversion line to the data for the dashed line at 362 mV shows it to be a poor choice. The shape factor plot shows much bigger excursions of the high energy points from a horizontal line for $\Delta E_0 = \pm 1$ keV. The 3-keV disparity is of little consequence in this investigation.

The small deviation from the allowed singles shape (above 15 keV) seen most clearly in the shape factor plot deserves comment. Other studies[5] have used thinner source backings than our 50 μg/cm^2 but our retarded ion beam (200 eV) isotope-separator-deposition method clearly gives purer, more uniform sources with less extraneous mass and, most important, reduced surface agglomeration, compared with solution- or vapor-deposited sources. In one earlier reported spectrum[17] there is indication of a similar down turn in the Kurie plot toward low energy but above 30 keV similar to that seen in Fig. 7(a). No such shape is seen in our ^{151}Sm ($E_0 = 77$ keV) or ^{89}Sr ($E_0 = 1.47$ MeV) spectra, run similarly and involving equal or larger efficiency and dead time corrections. Similarly as for the end point, the small allowed shape singles deviation (~6%) is not important to the SO shape study; on the scale of the uncertainties of our measurement of the K shaking spectrum shape, this much deviation has an al-

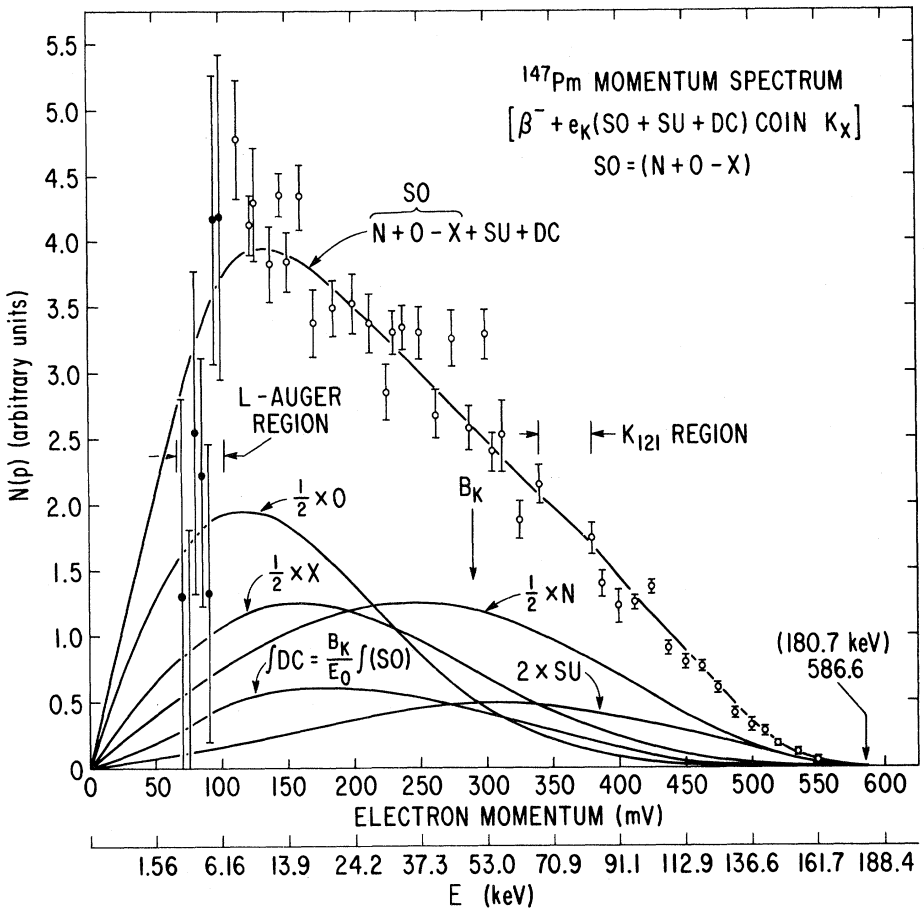

FIG. 8. ^{147}Pm K shaking plus direct collision momentum spectrum. The separate terms of Law-Campbell theory, nuclear (N), K orbital (O), and cross (X) are shown at half scale, and shakeup (SU) at twice relative scale. The DC relativistic shape is shown with relative intensity $DC/SO = B_K/E_0 = 0.21$ and the sum $N+O-X+SU+DC$ is normalized to the data near 250 mV by least-squares fitting. The solid experimental points in the region of the Sm L-Auger "line" are obtained from the $K\beta$ x ray intensity only, $\times 5.0$.

most negligible effect. We ignored the allowed shape deviation in the K shaking theory calculations that will be compared with experiment.

B. K x-ray coincidence spectrum

1. Resolution of components

In Fig. 6 a smooth interpolation under the K internal conversion [Eq. (3)] and L-Auger [Eqs. (6) and (7)] peaks gave the continuum. Using only coincidences with the $K\beta$ x rays and multiplying by a $K_x/K\beta$ ratio of 5.0 eliminated the L-Auger peak, but was statistically poorer (see Fig. 8). Also the shape of the L-Auger composite unresolved "peak" was used to aid in its delineation and "peeling." This was calculated by convoluting the theoretical Auger spectrum with the spectrometer resolution function (the K line shape). Next the contribution to the SO continuum by inner β group coincidences with K x rays was subtracted. The inner group forbidden spectrum shape ($\log ft = 10.5$) measured in coincidence with the 121.2-keV γ rays (Fig. 6) was subtracted with an intensity equal to the area of the peeled-off K internal conversion peak, as seen from the equality of Eqs. (3) and (4). A check on this intensity giving acceptable agreement was afforded by the ratio of Eqs. (3) and (5) for the K line and inner group coincidences (see below). The shape and intensity of the inner group contribution is indicated in Fig. 6.

2. Shaking probability P_K

Relative areas of the various electron components from the coincidence and singles measurements (the low energy singles rise below 15 keV was not included in extrapolating the momentum plot to zero momentum) are listed in Table I. Various intercomparable values of P_K, $\alpha_K(121)$, and $f_\gamma = f/(1+\alpha)$ can be calculated by pairwise comparisons of these data, using the equations of Sec. III F. and the labeled areas of Table I. The uncertainties quoted in Table I include both statistical and systematic contributions and should be interpreted as standard deviations.

(a) The most direct value for P_K comes from the ratio of Eq. (2) (area b–area c) to Eq. (1) (area a) which gives

$$P_K = \frac{A(\mathrm{SO}; K_x(\mathrm{SO}))}{A(\mathrm{singles})} \frac{1}{1.93} \frac{1}{\omega_K} \frac{1}{\epsilon_{Kx}} = (8.3 \pm 1.0) \times 10^{-5},$$

where $\omega_K = 0.94$, and $\epsilon_{Kx} = 0.07 \pm 0.007$ includes the source-Ge(Li) solid angle.

(b) Another value for P_K based on the ratio of Eq. (2) (area b–area c) to Eq. (3) (area c) gives

$$P_K = \frac{A(\mathrm{SO}; K_x(\mathrm{SO}))}{A(K\ \mathrm{line}; K_x(\mathrm{IC}))} \frac{f}{1+\alpha} \frac{\alpha_K}{1.93} = (8.5 \pm 0.8) \times 10^{-5},$$

where $f/(1+\alpha) = (2.9 \pm 0.1) \times 10^{-5}$ (McConnon[18]) and $\alpha_K = 0.826$ calculated (tables of Hager and Seltzer[19]) for 89% $M1$ + 11% $E2$ for the 121.2-keV transition.[4]

(c) A final correlated P_K value based on the ratio of Eq. (2) to Eq. (5) (area d) gives

$$P_K = \frac{A(\mathrm{SO}; K_x(\mathrm{SO}))}{A(\mathrm{inner}\ \beta; 121\gamma)} \frac{f}{1+\alpha} \frac{\epsilon_{121}}{\epsilon_{Kx}} \frac{1}{1.93} \frac{1}{\omega_K} = (9.6 \pm 1.2) \times 10^{-5},$$

where $\epsilon_{121}/\epsilon_{Kx} = 0.50 \pm 0.03$ was measured for our Ge(Li).

Although P_K also appears in Eq. (6) involving the L-Auger electrons, the uncertainties associated with the electron detection efficiency at these low energies (main component at 4.5 keV) gave P_K values which were not as reliable due to correction factors as large as 2. As an example of the validity of the various corrections in the L-Auger region, the following ratio gives

$$\frac{A(L\text{-Auger}; K_x(\mathrm{SO}+\mathrm{IC}))}{A(K\ \mathrm{line}; K_x(\mathrm{IC})) + A(\mathrm{SO}; K_x(\mathrm{SO}))/1.93} = 0.51 \pm 0.06,$$

about 20% low compared with the "theoretical" value of 0.633 for the curly brackets in Eqs. (6) and (7). This disparity, among others, leads us to discount the spectrum shape data below ~5 keV.

All of these values show internal consistence.

TABLE I. Relative areas determined experimentally for the various momentum distributions.

Label	Equation	Distribution	Relative area
a	(1)	A(singles)	$(1.222 \pm 0.030) \times 10^8$
b	(2)+(4)	A(SO+innerβ; K_x(SO+IC))	$(1.467 \pm 0.073) \times 10^3$
c	(3)	A(K line; K_x(IC))	$(1.86 \pm 0.13) \times 10^2$
d	(5)	A(innerβ; 121γ)	$(1.07 \pm 0.09) \times 10^2$
e	(6)+(7)	A(L-Auger; K_x(IC+SO))	$(4.37 \pm 0.44) \times 10^2$

We conclude that our best value for $P_K = (8.7 \pm 0.7) \times 10^{-5}$; the average of two previous measurements[4] is $9.0 \pm 0.9 \times 10^{-5}$. The Law-Campbell theory[4] gives $P_K(\mathrm{SO+SU}) = 7.71 \times 10^{-5}$ and $P_K(\mathrm{SO+SU+DC}) = 9.32 \times 10^{-5}$. Our P_K value alone thus gives no clear evidence on a DC component.

3. α_K and $f/(1+\alpha)$ values

The ratio of Eq. (3) to Eq. (1) gives

$$\alpha_K = \frac{A(K\text{ line}; K_x(\mathrm{IC}))}{A(\mathrm{singles})} \frac{1}{\omega_K} \frac{1}{\epsilon_{Kx}} \frac{(1+\alpha)}{f} = 0.80 \pm 0.10,$$

compared with 0.826 from the multipole admixture.

Alternatively, solving for $f/(1+\alpha)$, using $\alpha_K = 0.826$ as above in this ratio gives

$$f/(1+\alpha) = (2.80 \pm 0.35) \times 10^{-5}.$$

Similarly the ratio of Eq. (3) to Eq. (5) gives

$$\alpha_K = \frac{A(K\text{ line}; K_x(\mathrm{IC}))}{A(\mathrm{inner}\,\beta; 121\gamma)} \frac{\epsilon_{121}}{\epsilon_{Kx}} \frac{1}{\omega_K} = 0.92 \pm 0.12,$$

and finally the ratio of Eq. (5) to Eq. (1) gives

$$f/(1+\alpha) = \frac{A(\mathrm{inner}\,\beta; 121\gamma)}{A(\mathrm{singles})} \frac{1}{\epsilon_{121}} = (2.50 \pm 0.37) \times 10^{-5},$$

where $\epsilon_{121} = 0.035 \pm 0.004$. From this one gets $f = (5.7 \pm 0.7) \times 10^{-5}$ and $\log ft = 10.5$ for the inner group.

Again these values are internally consistent.

4. K SO spectrum shape; theory and experiment

While the P_K value agrees well with theory and other measurements, the primary thrust of these measurements has been to determine spectrum shapes. We digress to present some details of the Law-Campbell (L-C) theory[4] of K shaking in β decay that are essential to the analysis of the experiment. In L-C theory, the composite negatron (K electron plus nuclear β ray) momentum shakeoff spectrum for a transition exhibiting an allowed shape for the singles spectrum is given by

$$\lambda(p)dp = \frac{G_V^2 \xi}{4\pi^3} p^2 dp \int_0^{s_0(p)} \frac{s^2 ds}{2\pi^2} (W_K - E_p - E_s)^2 2\{|\langle e_s'|e_K\rangle|^2 F(Z', E_p) + |\langle e_p'|e_K\rangle|^2 F(Z', E_s) - |\langle e_s'|e_K\rangle||\langle e_p'|e_K\rangle|[F(Z', E_s)F(Z', E_p)]^{1/2}\}. \quad (8)$$

G_V and G_A are vector and axial vector coupling constants, $\langle 1\rangle^2$ and $\langle\sigma\rangle^2$ denote the corresponding nuclear matrix elements of allowed beta decay, and $\xi = \langle 1\rangle^2 + (G_A/G_V)^2\langle\sigma\rangle^2$. λ is the relative probability that one of the two ejected indistinguishable electrons has momentum p; the other has momentum s. Thus p and s enter the formula symmetrically, prior to the indicated integration. For a given electron ejected with momentum p, the integral limit $s_0(p)$ is the maximum momentum the other electron could have, i.e., when the antineutrino momentum is zero. In the antineutrino energy factor $(W_K - E_p - E_s)^2$, W_K is the total decay energy minus B_K, and E_j are ejected electron energies. The $F(Z', E_j)$ are Fermi functions accounting for the effect of the final nuclear Coulomb field ($Z' = Z+1$) on the free electrons, and $\langle e_j'|e_K\rangle$ are overlap integrals between the initial K-electron and the final electron continuum wave functions. L-C approximate the K shell state with relativistic hydrogenic wave functions.[4]

The most important features to consider when comparing this completely antisymmetrized theory with the experimental spectrum above are the three terms within the curly brackets. While all three terms in principle span the entire allowed energy range, zero to $E_0 - B_K$, the first term (after integration) rather closely follows the usual β spectrum (but with maximum energy decreased by B_K) and is prominent at higher energies; it is referred to as the nuclear component (N). The second term is predominant at the lower electron energies near B_K; it is called the orbital component (O), in analogy to the component of simple wave function overlap theory, since its energy dependence is governed mainly by the sharp dropoff in the atomic matrix element (wave function overlap integral) $\sim (E/B_K)^{-7/2}$. The final (negative) "cross" (X) term arises from the interference of the two final state free electrons, and hence is strong in the region of maximum overlap of the first two terms, where they have similar energies. The N and O term integrals are necessarily of equal intensity for all decay energies E_0. Since they overlap little for $E_0 \gg B_K$, the X term is then relatively small. The N and O terms (components) can then be easily distinguished,[1] as in ^{143}Pr ($E_0/B_K = 21$), and the small influence of the X term can be seen in the "valley" between them. Where $E_0 \to B_K$, the N, O, and X terms become very similar, in shape and in magnitude, as in ^{151}Sm.[3] ^{147}Pm, with $E_0/B_K = 4.9$, is an intermediate case in which the separate term influences are smoothly melded but with each prominent in different spectral re-

gions. These three principal components of the SO spectrum calculated for ^{147}Pm from the formulas of Ref. 4 are shown in Fig. 8 (at half scale) plus the SU component (shown at twice its 9% relative intensity) and the DC component (shown at the Feinberg intensity). SU, of course, contains only one free electron whereas the three SO terms, N + O − X, in sum represent two free electrons, as does the DC component. The SU shape is given[4] by an expression similar to Eq. (8).

In a perhaps more familiar representation, the energy spectrum of the experimental and theoretical shaking distributions are given in Fig. 9, calculated from $N(E)dE = N(p)dp$.

In both these figures the fit of the theoretical shape to the data is excellent over the entire energy range above ~5 keV. An essentially equally good fit is had without including a DC component (see Fig. 10). The necessity to include the interference (X) term is made clear, particularly in the range 125–350 mV, by an attempt to fit the data with (N+O+SU+DC) only; this curve, normalized to the data above 400 mV, was above the experimental average by ~20% at 150 mV. The misfit of the statistically poor, $K\beta$ only, data points at the extreme low end, near 5 keV, is due to a breakdown in the electron detection efficiency procedure there, and is not indicative of a weakness in the theory.

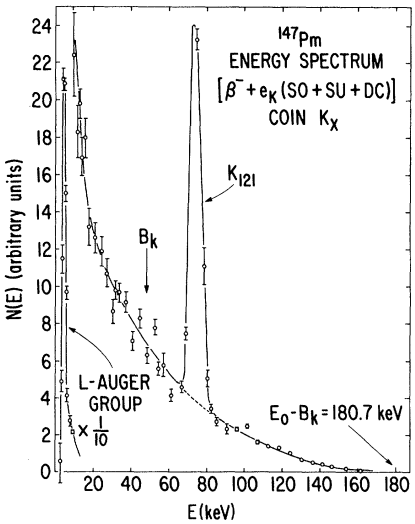

FIG. 9. ^{147}Pm K shaking plus direct collision energy spectrum. See Fig. 8. The K_{121} and L-Auger lines are retained to show their expected appearance in a scintillation spectrometer SO measurement (Ref. 7), albeit at poorer resolution.

5. Direct collision component

Calculation of the magnitude and shape of the direct collision (DC) contribution[20,4] is much less reliable, no complete theory having been developed without involving major approximations.[4] Feinberg[20] estimated that DC/SO (intensity) $\sim B_K/E_0$, or 21% for the ^{147}Pm decay. The intensity of DC which could be accommodated in the experimental spectrum shape was tested using the ratio (shape factor) plot of the experimental spectrum to the

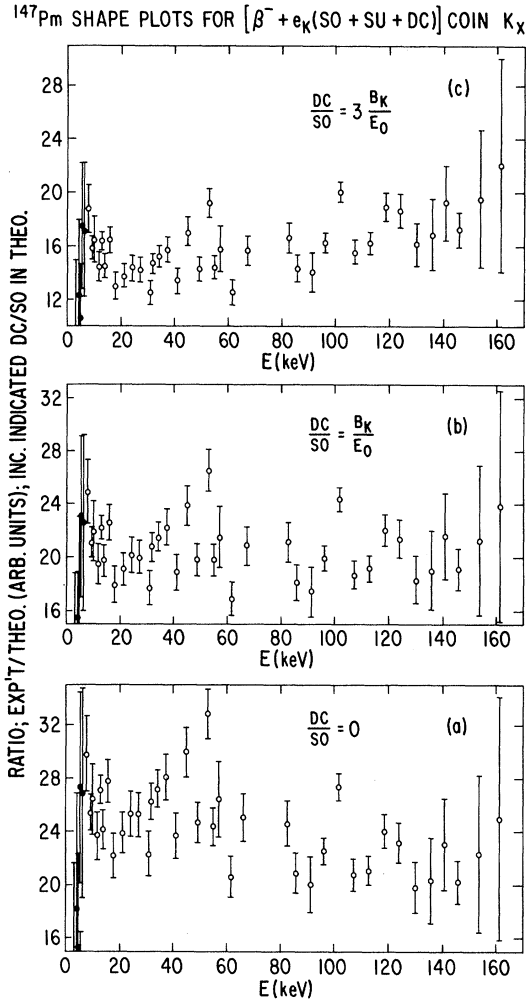

FIG. 10. Shape factor plots (ratio of experimental to theoretical intensity) for K-electron ejection in ^{147}Pm β decay, with varying (indicated) relative amounts of DC included in the theory with SO+SU: in (a), no DC; in (b), the Feinberg estimate, $DC/SO = B_K/E_0 = 0.21$; in (c), 3 times the Feinberg estimate. An energy-independent ratio, i.e., points along a horizontal line, indicates agreement of measurement with theory. Plot (c) indicates 3× Feinberg estimate is an upper limit for DC component.

theoretical (SO+SU) contributions with varying amounts of DC added; see Fig. 10. The DC shape used was calculated from Feinberg's prescription, as in Paper I on ^{143}Pr, and is shown in Fig. 8. However, for ^{147}Pm with a fourfold higher B_K/E_0 ratio, the DC shape is much more similar to that of (SO+SU) than for the high energy case of ^{143}Pr; despite the expected much larger DC contribution in the former case, the shape similarity results in a comparable sensitivity of the measured shape to the DC component, in each case. Figure 10 shows the results of these tests where no DC contribution was added to the L-C theory in (a), the Feinberg estimate added in (b) (as in Figs. 8 and 9), and 3 times the Feinberg estimate added in (c). The criterion for agreement of experiment and theory is an energy-independent ratio. From the slope and shape of plot (a) we conclude that the spectrum shape is consistent with no DC component, and (c) rejects any such contribution exceeding 3 times the Feinberg prediction, ~60%. Our DC upper limit firmly rejects the recent proposal of Isozumi *et al.*[8] that DC/SO~1. This reinforces the same, even more stringent limitation on the DC contribution obtained[21] for the case of ^{151}Sm (in that case from the P_K value) in which the DC component could not exceed $\frac{1}{4}$ of the Feinberg estimate, and the conclusion from several recent P_K measurements,[2,4,22] which match better the L-C SO+SU predictions with no DC.

Finally, the principal conclusions to be drawn are that the data indicate an excellent fit to L-C theory in P_K and in shape, to ~5 keV, only around $\frac{1}{9}$ of B_K; that the large negative contribution of the interference term is clearly required for this fit; and that the residual theoretical approximations, the sudden approximation, no initial state correlation, and hydrogenic wave functions, are all adequate for K shaking in ^{147}Pm.

ACKNOWLEDGMENTS

Two of the authors (G.S. and D.A.B.) wish to acknowledge support by the Center for Educational Affairs and by the Chemistry Division of ANL. We thank Jerome Lerner for the isotope separator source deposition, Ruth Sjoblom for the chemical purification, Frank Wagner for computational assistance, James Law for discussions and check calculations of shaking spectrum shapes and probabilities, and Paul Stephas for communications on direct collision calculations.

---

*Visiting professor on sabbatical leave from University of Missouri, Columbia, Missouri, 1971–1972.
†Work performed under the auspices of U.S.E.R.D.A.
‡Present address: 420 Brewster Avenue, Lombard, Illinois 60148.
§Visiting professor on sabbatical leave from Buffalo State College, Buffalo, New York.

[1]M. S. Freedman, Ann. Rev. Nucl. Sci. 24, 209 (1974).
[2]H. J. Fischbeck, F. Wagner, F. T. Porter, and M. S. Freedman, Phys. Rev. C 3, 265 (1971).
[3]The ^{143}Pr study of Ref. 2; the present ^{147}Pm case; and completed studies of the extreme low energy case, ^{151}Sm, of the unique first forbidden transition ^{89}Sr, and of the extreme deviant from the allowed shape, ^{210}Bi. The latter three will soon be submitted for publication. Perforce, reference is here made to them for certain experimental and analytical details pertinent also to the ^{147}Pm study, particularly the analysis of the electron detection efficiency.
[4]J. Law and J. L. Campbell, Nucl. Phys. A185, 529 (1972); J. L. Campbell and J. Law, Can. J. Phys. 50, 2451 (1972); J. Law and J. C. Campbell, Phys. Rev. C 12, 984 (1975).
[5]J. H. Hamilton, L. M. Langer, and W. B. Smith, Phys. Rev. 112, 2010 (1958).
[6]A. J. Mord, in Proceedings of the International Conference on Inner Shell Ionization Phenomena, Oak Ridge, Tennessee, 1972, edited by R. W. Fink *et al.* (unpublished), p. 2079 [USAEC-CONF(720404)].
[7]P. Stephas and B. Crasemann, Phys. Rev. 164, 1509 (1967).
[8]Y. Isozumi and S. Shimizu, Phys. Rev. C 4, 522 (1971); Y. Isozumi, T. Mukoyama, and S. Shimizu, Phys. Rev. Lett. 29, 298 (1972).
[9]W. B. Ewbank, M. J. Martin, and S. Raman, Nucl. Data B2, No. 4 (1967).
[10]F. T. Porter, M. S. Freedman, T. B. Novey, and F. Wagner, Jr., Phys. Rev. 103, 921 (1956).
[11]F. T. Porter and P. P. Day, Phys. Rev. 114, 1286 (1959).
[12]F. T. Porter, M. S. Freedman, F. Wagner, Jr., and I. S. Sherman, Nucl. Instrum. Meth. 39, 35 (1966).
[13]All magnetic spectrometers give linear momentum (p) rather than linear energy analysis, and have a variable window width Δp proportional to p; thus, reduction of the "rate" spectrum to a "momentum" spectrum requires division by $\Delta p \propto p \propto mV$.
[14]Electron momentum p, in m_0c units, is given by $p = 0.001\,555$ mV.
[15]W. Bambynek, B. Crasemann, R. W. Fink, H.-U. Freund, H. Mark, C. D. Swift, R. E. Price, and P. V. Rao, Rev. Mod. Phys. 44, 716 (1972).
[16]F. T. Porter, M. S. Freedman, T. B. Novey, and F. Wagner, Jr., Argonne National Laboratory Report No. ANL-5525 (unpublished).
[17]H. Agnew, Phys. Rev. 77, 655 (1950).
[18]D. McConnon, Int. J. Appl. Radiat. Isot. 22, 253 (1971).
[19]R. S. Hager and E. C. Seltzer, Nucl. Data A4, 1 (1968).
[20]E. L. Feinberg, Yad. Fiz. 1, 612 (1965) [Sov. J. Nucl. Phys. 1, 438 (1965)].
[21]M. S. Freedman and D. A. Beery, Phys. Rev. Lett. 34, 406 (1975).
[22]C. W. E. Van Eijk and R. W. Kooy, Phys. Lett. 46B, 351 (1973); H. H. Hansen, Phys. Rev. 14, 281 (1976).